Kinetic Characterization of Adenylosuccinate Synthetase from the Thermophilic Archaea *Methanocaldococcus jannaschii*†

Sonali Mehrotra and Hemalatha Balaram*

Molecular Biology and Genetics Unit, Jawaharlal Nehru Centre for Advanced Scientific Research, Jakkur Post, Bangalore 560064, India

Received May 24, 2007; Revised Manuscript Received August 29, 2007

ABSTRACT: Adenylosuccinate synthetase (AdSS) catalyzes the Mg^{2+} dependent condensation of a molecule of IMP with aspartate to form adenylosuccinate, in a reaction driven by the hydrolysis of GTP to GDP. AdSS from the thermophilic archaea, *Methanocaldococcus jannaschii* (MjAdSS) is 345 amino acids long against an average length of 430−457 amino acids for most mesophilic AdSS. This short AdSS has two large deletions that map to the middle and C-terminus of the protein. This article discusses the detailed kinetic characterization of MjAdSS. Initial velocity and product inhibition studies, carried out at 70 °C, suggest a rapid equilibrium random AB steady-state ordered C kinetic mechanism for the MjAdSS catalyzed reaction. AdSS are known to exhibit monomer−dimer equilibrium with the dimer being implicated in catalysis. In contrast, our studies show that MjAdSS is an equilibrium mixture of dimers and tetramers with the tetramer being the catalytically active form. The tetramer dissociates into dimers with a minor increase in ionic strength of the buffer, while the dimer is extremely stable and does not dissociate even at 1.2 M NaCl. Phosphate, a product of the reaction, was found to be a potent inhibitor of MjAdSS showing biphasic inhibition of enzyme activity. The inhibition was competitive with IMP and noncompetitive with GTP. MjAdSS, like the mouse acidic isozyme, exhibits substrate inhibition, with IMP inhibiting enzyme activity at subsaturating GTP concentrations. Regulation of enzyme activity by the glycolytic intermediate, fructose 1,6 bisphosphate, was also observed with the inhibition being competitive with IMP and noncompetitive against GTP.

The de novo biosynthesis of AMP from IMP involves two steps, with the first step catalyzed by adenylosuccinate synthetase (AdSS[1]) followed by adenylosuccinate lyase catalyzing the second step. AdSS catalyzes the formation of succinyl AMP (sAMP) from IMP through a concerted Mg^{2+} dependent two step process, where the first step involves the transfer of γ-phosphate from GTP to IMP resulting in the formation of the intermediate, 6-phosphoryl IMP. Subsequent nucleophilic attack by the α-amino group of aspartate on the C6 position of the phosphorylated purine results in displacement of phosphate and generation of the products sAMP, GDP, and P_i (*1*−*4*). All well characterized AdSS have been shown to function as homodimers (*5*, *6*). The sequence length of AdSS from many bacteria and eukaryotes is similar, ranging from 430 to 457 amino acids (*7*) with an identity of 30−40% across sequences. Plant chloroplast AdSS differ in having an amino terminal extension that serves as the signal peptide for targeting the enzyme to the organelle (*8*, *9*). *Leishmania major* has a significantly longer AdSS with 710 amino acids, and the experimentally determined molecular mass of *L. donovani* enzyme is >250,000 Da (*10*). However, the significance of the additional amino acids in context of the protein structure and function has not been determined. Vertebrates have two AdSS genes coding for proteins of similar molecular mass that are referred to as acidic and basic isozymes on the basis of their pI values (*11*). The two proteins exhibit 75% identity in sequence, with the acidic enzyme that is present in most tissues involved in AMP synthesis and the basic AdSS expressed largely in muscle, mediating oxo-purine cycling (*12*). The structures of AdSS from *E. coli*, mouse, arabidopsis, and *Plasmodium falciparum* are highly conserved, comprising multiple subdomains (*9*, *13*−*15*). The structures consist of a central β sheet formed by nine parallel and one antiparallel β strand. Of the four subdomains that border the central sheet, subdomains I, III, and IV contribute the majority of the residues forming the ligand binding pocket. The intersubunit interface mainly comprises residues from subdomain II and helices α11−α13 that do not belong to any domain (*15*).

Though the AdSS sequence from a vast majority of organisms is 430−457 amino acids in length, the NCBI protein data base contains 23 annotated AdSS sequences that are shorter in length by 90−120 amino acids. Of these, 21 belong to archaea and 2 to bacterial species. The first report

† This work was supported by Council of Scientific and Industrial Research, India. S.M. was supported by a Senior Research Fellowship from the Council of Scientific and Industrial Research, India.

* Corresponding author. Tel: 91-80-22082812. Fax: 91-08-22082766. E-mail: hb@jncasr.ac.in.

[1] Abbreviations: AdSS, adenylosuccinate synthetase; MjAdSS, *Methanocaldococcus jannaschii* adenylosuccinate synthetase; PhAdSS, *Pyrococcus horikoshii* adenylosuccinate synthetase; IMP, inosine monophosphate; GMP, guanosine monophosphate; GDP, guanosine diphosphate; GTP, guanosine triphosphate; AMP, adenosine monophosphate; sAMP, succinyl AMP or adenylosuccinate; Asp, aspartate; F16BP, fructose 1,6 bisphosphate; 6P-IMP, 6-phosphoryl IMP; MES, 2-morpholinoethanesulfonic acid.

10.1021/bi701009y CCC: $37.00
Published on Web 10/11/2007

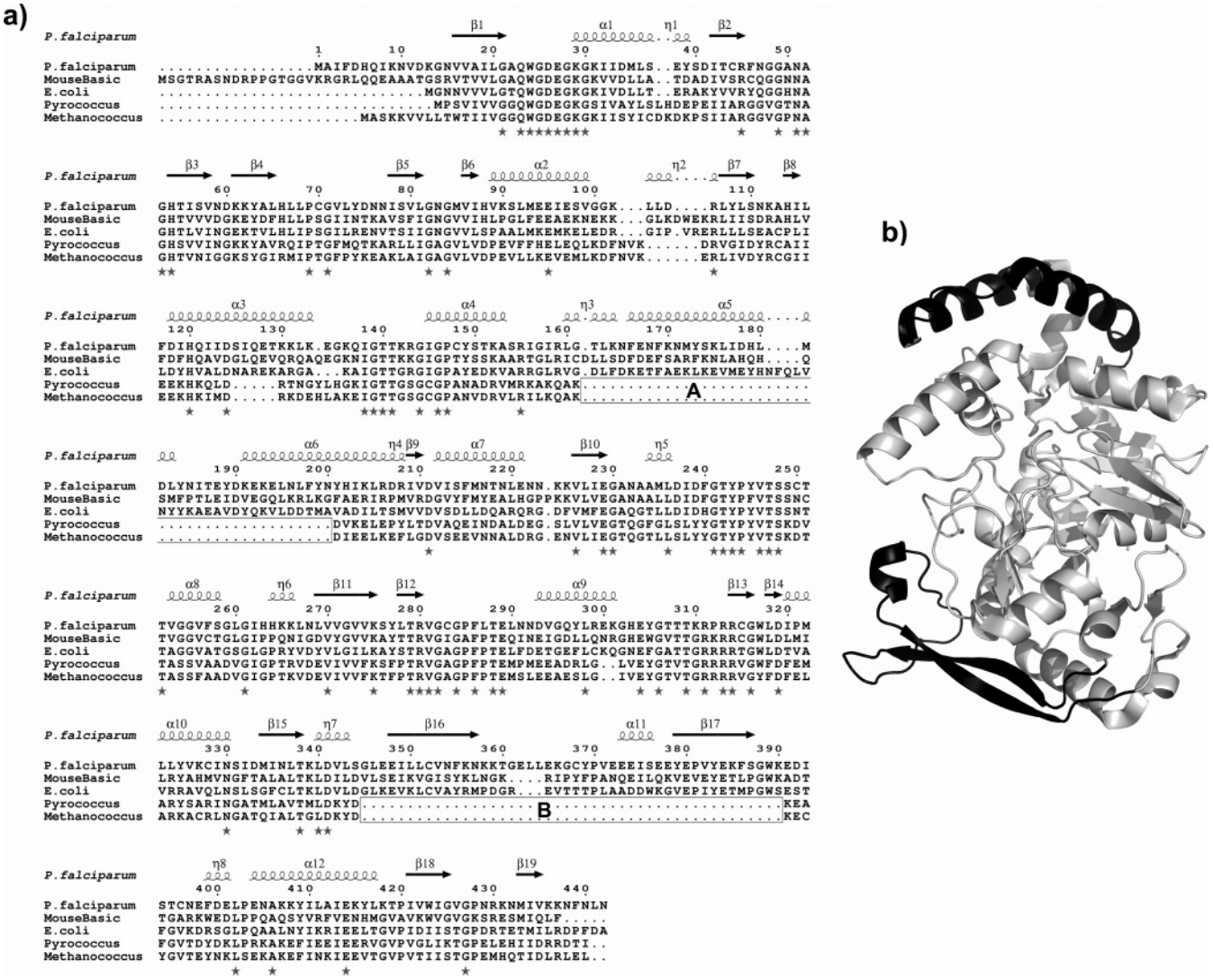

FIGURE 1: (a) Alignment of amino acid sequences of adenylosuccinate synthetase. The alignment was carried out using CLUSTALW and was adorned with secondary structure elements using ESPript (*58*). The sequence numbering and secondary structure assignments on the top correspond to the *P. falciparum* AdSS (PfAdSS) sequence. α, represents alpha helices; *η*, represents 3_{10} helices; *β*, represents sheets, and stars mark conserved residues. Boxed regions (A and B) highlight the deletions in *Pyrococcus* and *Methanococcus* AdSS sequences. (b) Ribbon representation of PfAdSS monomer. Marked in black are the segments deleted in MjAdSS. The figure was generated using PyMOL (*59*).

of a short AdSS sequence was from the *Pyrococcus* species strain ST700 (*16*) followed by that from *Pyrococcus furiosus* (*17*). The short AdSS sequences consist of 333−345 amino acids. Figure 1a shows the multiple sequence alignment of the short AdSS sequences from *Methanocaldococcus jannaschii* and *P. furiosus* with the longer homologues from *P. falciparum*, *E. coli*, and mouse. The short AdSS sequences are characterized by 2 major deletions (labeled A and B, respectively in Figure 1a) that map to the mid-region and C-terminus of the protein. The loss of segment A leads to the loss of α 5, 6, and *η* 3 from subdomain II, while the loss of segment B results in the deletion of *β* 16, 17, and α 11 that form part of subdomain IV (Figure 1a and b). The effect of these deletions on the structure, function, and regulation of AdSS has not been examined.

Fromm and co-workers elucidated the kinetic mechanism of the three-substrate reaction catalyzed by *E. coli* AdSS. This enzyme from initial velocity and product inhibition kinetics was found to follow a sequential rapid equilibrium random mechanism (*18*). Equilibrium isotope exchange studies highlighted a random sequential model for rat muscle AdSS (*19*), whereas product inhibition studies on *P. falciparum* AdSS yielded line patterns in the double reciprocal plots indicative of a fully ordered mechanism, with IMP binding preceding GTP, followed by aspartate binding to the E-IMP−GTP complex (*20*). In this article, we report on the initial velocity studies in the absence and presence of competitive inhibitors carried out to elucidate the overall kinetic mechanism of *M. jannaschii* AdSS. The present work is the first report of an AdSS that exhibits dimer−tetramer equilibrium. All AdSS have been reported to show monomer−dimer equilibrium, and this feature has been implicated in the regulation of enzyme activity (*6*). The thermophilic synthetase, like the mouse AdSS, is inhibited by both IMP and fructose 1,6 bisphosphate (F16BP) (*12*). Our studies also show that phosphate (Pi) is a potent inhibitor of MjAdSS. Upon varying the concentration of Pi, biphasic inhibition of enzyme activity was observed, indicating the presence of two distinct phosphate binding sites on MjAdSS.

EXPERIMENTAL PROCEDURES

Chemicals. All media components were purchased from HiMedia Laboratories (Mumbai, India). Pfx polymerase was procured from Invitrogen (California), restriction enzymes, and T4 DNA ligase were from Bangalore Genei Pvt. Ltd., (Bangalore, India) and oligonucleotides from Microsynth AG (Balgach, Switzerland). Substrates and inhibitors used in kinetic studies and protein markers were from Sigma Chemical Company (St.Louis, MO). Hadacidin was obtained from Developmental Therapeutics Program, National Cancer Institute, NIH, Bethesda, MD. *Methanocaldococcus jannaschii* genomic DNA was purchased from ATCC (Manassas, USA). Akta Basic HPLC, sephadex G25, Q-sepharose, Sephacryl 200 and Superdex 200 were from Amersham Pharmacia (Uppsala, Sweden). All assays were conducted using a Hitachi U2010 (Hitachi High-Technologies Corporation, Tokyo, Japan) spectrophotometer fitted with a water circulated cell holder. MALDI-MS spectra of the protein were recorded on an Ultraflex II TOF/TOF mass spectrometer (Bruker Daltonics, Bremen, Germany).

MjAdSS Cloning and Purification. The open reading frame encoding MjAdSS was PCR amplified from *M. jannaschii* genomic DNA using forward 5′ TAT***CCATGG***CTAGCAAAAAGGTGGTTTTATTGACTTGC 3′ and reverse 5′ TGC***GGATCC***TTATAGCTCGAGTCTTAAATCAATTGTTTGGTG 3′ primers. The sequences in bold indicate *Nco*1 and *Bam* H1 restriction sites that were used to clone the gene into pET 23d expression vector (Novagen, Madison, USA). The protein was expressed in *E. coli* BL21 (DE3) cells that were grown at 37 °C for 10 h. The cells were harvested by centrifugation, resuspended in lysis buffer (50 mM Tris HCl at pH 7.4, 10% glycerol, 300 mM NaCl, 0.2 mM PMSF, and 2 mM DTT) and lysed using a French press. After the separation of debris, the supernatant was first treated with 0.01% polyethylenimine to remove nucleotides and then subjected to thermal precipitation at 70 °C for 10 min. This was followed by 40% and then 75% ammonium sulfate precipitation. The protein pellet was dissolved in 20 mM Tris HCl at pH 6.9, 10% glycerol, 2 mM DTT, and 0.1 mM PMSF and desalted on a sephadex G-25 column equilibrated with the same buffer. The desalted protein was put through Q-sepharose anion exchange chromatography. The protein was eluted using a linear gradient of NaCl with buffer A (20 mM Tris HCl at pH 6.9, 10% glycerol, 1 mM DTT, and 0.1 mM PMSF) as solvent system and was found to elute between 250 and 280 mM NaCl. The fractions containing the protein were pooled, concentrated, and further purified through sephacryl 200 gel filtration chromatography (20 mM Tris HCl at pH 7.4, 10% glycerol, 1 mM EDTA, 0.1 mM PMSF, and 2 mM DTT). The samples were analyzed by SDS−PAGE (*21*), and pure fractions were concentrated and stored at −20 °C. The protein concentration was estimated by the method of Bradford (*22*) using BSA as standard. To obtain the mass spectrum of MjAdSS, the protein was extensively dialyzed against distilled water to remove all additives. One microliter of the protein sample at 4.2 mg/mL concentration was mixed with 1 μL of sinapinic acid prior to spotting on target plate. Spectra were acquired in positive ion mode.

Size Exclusion Chromatography. Size exclusion chromatography was carried out on an analytical Superdex 200 (1 cm × 30 cm) column attached to Akta Basic HPLC using 20 mM Tris HCl at pH 7.4 as the solvent system. The runs were performed at 0.5 mL min^{-1}, and the protein elution was monitored simultaneously at 280 and 220 nm. The column was calibrated with β-amylase (200 kDa), alcohol dehydrogenase (150 kDa), bovine serum albumin (66 kDa), carbonic anhydrase (29 kDa), and cytochrome *c* (12.4 kDa). To monitor the effect of NaCl, 18 μM protein was incubated with the appropriate concentration of salt for 30 min at room temperature and injected into a column prequilibrated with the same NaCl concentration in 20 mM Tris HCl at pH 7.4. To monitor the effect of ligand binding on the oligomeric status of MjAdSS, 12 μM protein was incubated with 2 mM magnesium acetate, 60 μM IMP, or 60 μM GTP in different combinations for 30 min at room temperature and chromatographed with the appropriate ligand in the running buffer. All chromatographic runs were performed at 25 °C.

Circular Dichroism Spectroscopy. Far-UV CD spectra of 5 μM MjAdSS in 20 mM Tris HCl at pH 7.4 and different concentrations of NaCl were recorded on a Jasco J-810 spectropolarimeter (JASCO Corporation, Tokyo, Japan) after preincubation of the protein at room temperature for 30 min with the appropriate concentration of NaCl. Spectra of suitable blanks were subtracted from the protein spectra.

Enzyme Assays. All assays were conducted at 70 °C using a water circulated cell holder fitted to a Hitachi U2010 spectrophotometer. The temperature was maintained with a Julabo F25 (JULABO Labortechnik GmbH, Seelbach, Germany) circulating water bath. The assays were performed in 30 mM MES at pH 6.5 (pH 6.0 at 70 °C) and 15 mM magnesium acetate with 0.65−0.85 μg of enzyme in a volume of 300 μL. The reaction mix preincubated at 70 °C for 30 s before initiation with GTP. The reaction rates were monitored as an increase in absorbance at 290 nm and $\Delta\epsilon$ of 3390 $M^{-1}cm^{-1}$ (*23*, *24*) was used to calculate the amount of product (sAMP) formed. For the determination of kinetic constants, IMP concentration was varied between 25 and 750 μM, GTP between 10 and 300 μM, and aspartate between 0.25 and 10 mM, while their concentrations when fixed were 500 μM, 250 μM, and 10 mM for IMP, GTP, and aspartate, respectively. The data were analyzed by fitting to the Michaelis−Menten equation (eq 1) as follows:

$$v = V_{max}[S]/K_m + [S] \quad (1)$$

where v and V_{max} are the initial velocity and maximum velocity, respectively, K_m is the Michaelis constant, and S is substrate concentration.

pH Dependence of MjAdSS Kinetics. The effect of pH on enzyme activity was monitored at fixed substrate concentrations of 500 μM IMP, 250 μM GTP, and 10 mM aspartate. Acetate was chosen as buffer for the pH range 4−5, MES for the pH range 5.5−6.5, and Tris HCl for the pH range 7.0−8.5. The data were fit to eq 2 (BELL equation) (*25*) using GraphPad Prism, version 4 (GraphPad Software, Inc., San Diego, CA) as follows:

$$\log(y) = \log(c/(1 + H/K_1 + K_2/H)) \quad (2)$$

where y is the pH dependent parameter, c is the pH independent value of the parameter, [H] is the hydrogen ion

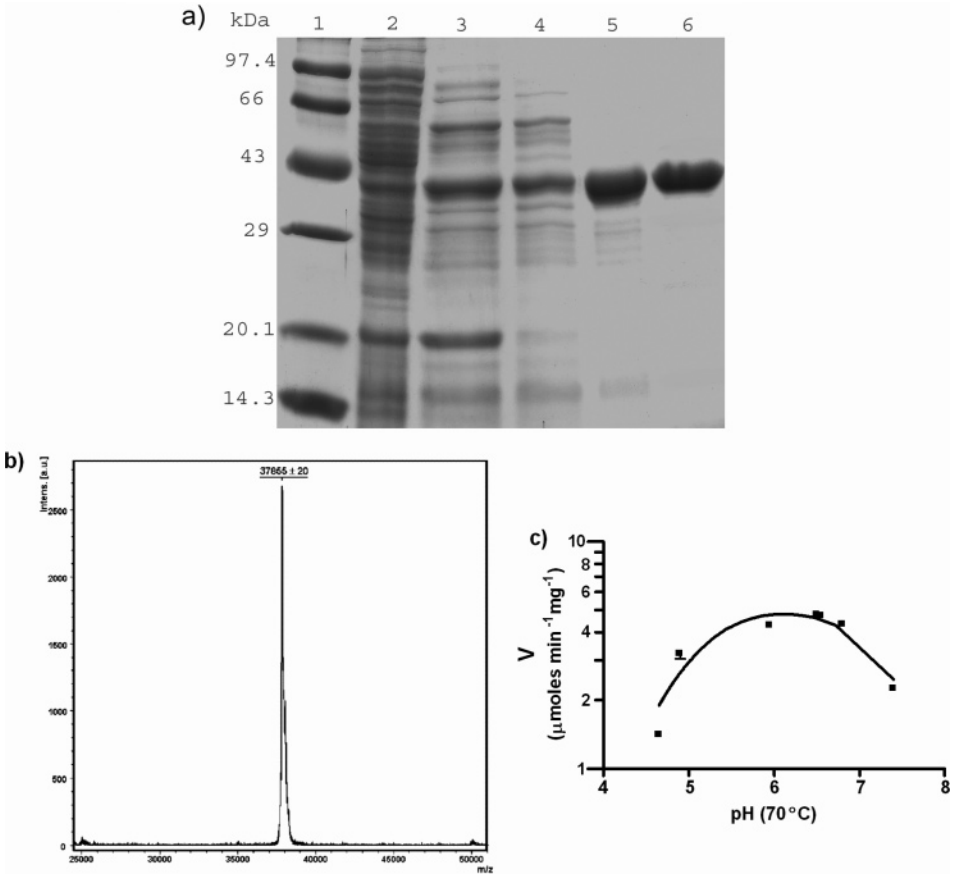

FIGURE 2: Purification and preliminary characterization of MjAdSS. (a) Electrophoretic analysis of the purification of recombinant MjAdSS. Lane 1, marker; lane 2, crude lysate; lane 3, supernatant after thermal precipitation; lane 4, precipitate from 70% ammonium sulfate fraction; lane 5, Q-sepharose purification; and lane 6, Sephacryl 200 fraction. (b) MALDI-MS spectrum of purified recombinant MjAdSS. (c) pH profile of MjAdSS activity. The pH values of buffers used were taken at 70 °C.

concentration, and K_1 and K_2 are the ionization constants for the two ionizable groups involved in catalysis.

Initial Velocity Measurement and Inhibition Studies. For the determination of initial velocity patterns, the concentration of one substrate was varied, keeping the concentration of the other two substrates in a fixed ratio at different levels in the range of their Michaelis constant. Initial rates were also measured by varying the concentration of one substrate at different fixed concentrations of the second substrate, with the third substrate held at saturating concentration.

Inhibition patterns with the products sAMP, GDP, and the aspartate analogue, hadacidin, were determined by measuring the initial rate at variable concentrations of one substrate, fixed subsaturating concentrations of the other two substrates, and at different fixed concentrations of the inhibitor. Inhibition studies with the nucleotides, AMP and GMP, were also done in a similar manner. Pi and F16BP inhibition studies were carried out by the method of Dixon (*26*), where the inhibitor concentration was varied at different fixed concentrations of one substrate with the other two substrates maintained at twice their K_m values. Substrate (IMP) inhibition was examined by measuring the initial rates at different fixed concentrations of GTP, with aspartate being held constant at 10 mM. The assay conditions were as described above, and the reactions were carried out at 70 °C. Concentrations of substrates and inhibitors used in specific assays are indicated in the figures or figure legends.

Data Analysis. All initial rate data were first analyzed by double reciprocal plots of velocity versus substrate concentration and associated secondary plots. Initial rate data of inhibition by Pi and F16BP were analyzed by $1/v$ versus [I] plots. The data were then fitted by nonlinear regression to standard kinetic models using GraphPad Prism, version 4. The best fit models were selected on the basis of goodness-of-fit (extra sum-of-squares F test) and *P* values. The kinetic parameters obtained by nonlinear regression analysis were in agreement with the values obtained by Lineweaver−Burk plots and related secondary plots.

RESULTS

Protein Expression, Purification and Preliminary Characterization. Methanocaldococcus jannaschii is an anaerobic thermophilic archaea. A BLAST search of the *M. jannaschii* genome using *E. coli* AdSS sequence as the query retrieved a protein sequence of 345 amino acids annotated as putative AdSS. For the purpose of generating recombinant MjAdSS, the gene was amplified from *M. jannaschii* genomic DNA, cloned into pET 23d expression vector and confirmed by DNA sequencing. The protein was expressed in the BL21 (DE3) strain of *E. coli* cells, which were grown at 37 °C, and since the level of leaky expression was high, induction with IPTG was omitted. Purification of the heat (70 °C) treated soluble fraction of the cell lysate using Q-sepharose anion exchange chromatography followed by gel filtration

Table 1: Comparison of Kinetic Parameters of MjAdSS with *P. falciparum*, *E. coli*, and Mouse AdSS

enzyme	k_{cat} (s^{-1})	K_m (μM)		
		IMP	GTP	aspartate
M. jannaschii[a]	4.2 ± 0.1	75.5 ± 4.6	42.6 ± 2.8	1079 ± 74
P. falciparum[b]	1.1 ± 0.03	23 ± 4	18.4 ± 2.0	1800 ± 50
E. coli[c]	1.0 ± 0.05	30 ± 0	26.2 ± 2.3	230 ± 40
Mouse (basic)[d]	5.4 ± 0.4	45 ± 7	12 ± 2	140 ± 20
Mouse (acidic)[e]	4.2 ± 0.4	12 ± 2	15 ± 2	950 ± 50

[a] The values were taken from the present study. [b] The values were taken from ref *20*. [c] The values were taken from ref *6*. [d] The values were taken from ref *12*. [e] The values were taken from ref *12*.

yielded protein of >95% purity (Figure 2a) as judged by SDS−PAGE. MALDI mass spectrometric analysis of the recombinant protein yielded a subunit molecular weight of 37855 ± 20 Da (Figure 2b). The predicted molecular weight based on its amino acid sequence is 38060 Da. Thus, the experimentally obtained mass corresponds to protein devoid of the first two amino acids, methionine and alanine. Similar mass was obtained with different batches of purified enzyme. The protein was stable at −20 °C without any drop in activity for atleast 6 months. Preliminary activity measurements under varied reaction conditions enabled the optimization of enzyme assay methodology. The protein showed a continuous increase in activity till 80 °C (data not shown). All kinetic studies reported in this article are from activity measurements performed at 70 °C in 30 mM MES at pH 6.5 and 15 mM magnesium acetate. Phosphate was found to be an inhibitor of enzyme activity, and hence, its use during protein purification and in assay solutions was avoided. pH dependence of enzyme activity (Figure 2c) when fitted to the BELL equation (eq 2) yielded pK_1 and pK_2 values of 4.92 and 7.33, respectively. In all AdSS, a conserved histidine and aspartic acid have been implicated to function as catalytic acid and base, respectively (*27*−*29*). These residues in MjAdSS correspond to His 51 and Asp 21.

K_m and k_{cat} values for MjAdSS obtained from initial rate data at saturating concentrations of two substrates with the third at variable concentration and fit to the Michaelis−Menten equation (eq 1) are summarized in Table 1. The K_m for IMP and GTP are in micromolar range, while that for aspartate is 1 mM. The k_{cat} for MjAdSS at 70 °C is 4.2 s^{-1}, which reduces to 0.45 s^{-1} at 25 °C.

Like all other AdSS, the *M. jannaschii* enzyme requires Mg^{2+} for catalysis with maximum activity obtained at 15 mM magnesium acetate (data not shown). The Mg^{2+} dependence of MjAdSS activity exhibits a Hill coefficient of 1, indicating the presence of only one Mg^{2+} binding site in each subunit, a feature similar to mouse acidic and basic isozyme (*12*). The crystal structures of liganded AdSS also contain one Mg^{2+} bound to α and β phosphoryls of GDP (*15*, *27*, *29*−*31*). However, kinetic analysis on the Mg^{2+} dependence of *E. coli* AdSS activity showed the involvement of two Mg^{2+} ions for each subunit. The second metal ion has been proposed to interact with the substrate aspartate in the enzyme active site (*24*).

Quaternary Structure of MjAdSS. The predicted subunit molecular mass of MjAdSS is 38 kDa. On a precalibrated Superdex 200 column, the protein eluted as a single peak at a volume of 13.0 mL, which corresponds to a mass of 112 kDa (Figure 3a). Repeated runs on calibrated Superdex 200 columns were highly reproducible with only minor variation in molecular mass ranging from 104 to 115 kDa. Variation in protein concentration from 10 to 0.96 μM did not lead to any change in elution profile (data not shown). However, on addition of 50 and 100 mM NaCl, the protein peak shifted to higher elution volumes of 14.0 mL and 14.2 mL, corresponding to a mass of 79 kDa and 70 kDa, respectively. Further increase in NaCl concentration up to 1.2 M did not lead to a significant change in retention volume (Figure 3a). The effect of salt on protein secondary structure monitored by circular dichroism spectroscopy showed no change in spectral pattern but for a minor increase in molar ellipticity at 220 nm (Figure 3c). MjAdSS contains two tryptophans per monomer. Examination of fluorescence spectra of MjAdSS, upon excitation at 290 nm, showed neither a shift in emission maximum nor a change in fluorescence intensity in the presence and absence of NaCl (data not shown). This indicates the absence of gross secondary and tertiary structural changes in the protein upon the addition of NaCl. The gel filtration profiles thus indicate that in the absence of NaCl, MjAdSS is an equilibrium mixture of dimers and tetramers. The presence of NaCl breaks the tetramer to dimers without further dissociation on increase in salt concentration. This is the first report of a homotetramer of AdSS. Essentiality of the homotetramer for enzyme activity was monitored by measuring activity in the presence of increasing salt concentration. The enzyme lost 30% activity at low NaCl concentration of 100 mM, while at 300 mM, only 25% of activity was retained (Figure 3d). Studies on mouse AdSS have shown that chloride ions inhibit enzyme activity (*12*), a feature not seen with MjAdSS because substitution of magnesium acetate with $MgCl_2$ in the assay mixture did not result in any change in enzyme activity (data not shown). Gel filtration chromatography in the presence of ligands also supported the essentiality of an association state higher than a dimer for activity. Inclusion of 2 mM magnesium acetate shifted the protein peak to a larger elution volume when compared to that of the unliganded protein. However, on addition of IMP and GTP in the presence of magnesium, the protein eluted at a lower retention volume and hence a higher oligomeric form, indicating that substrates mediate the association of MjAdSS dimers to form a tetramer (Figure 3b). This substrate driven shift to tetramer indicates that the catalytically active form of the enzyme at 70 °C could also be expected to be the higher oligomeric state, as the dimer-tetramer equilibrium would exist even at high temperature.

Kinetic Mechanism of MjAdSS. Initial Velocity Studies and Kinetic Parameters. The kinetic mechanism of *E. coli*, mouse, and *P. falciparum* AdSS that belong to the subfamily of long AdSS is well characterized (*18*−*20*). However, the short AdSS from thermophilic organisms have not been studied. Enzyme kinetic mechanisms can be modeled on rapid equilibrium or steady-state assumptions. Steady-state models invoke rate constants for the equilibrium between species in the kinetic scheme, and these are well derived for uni and bireactant systems (*32* (pp 139−170), *33*). However, in trisubstrate reactions, steady-state models lead to initial velocity equations with a large number of parameters that cannot be easily determined from kinetic studies. Rapid equilibrium assumptions reduce the number of constants in the rate equation (*32* (pp 209−241)). To deduce the kinetic

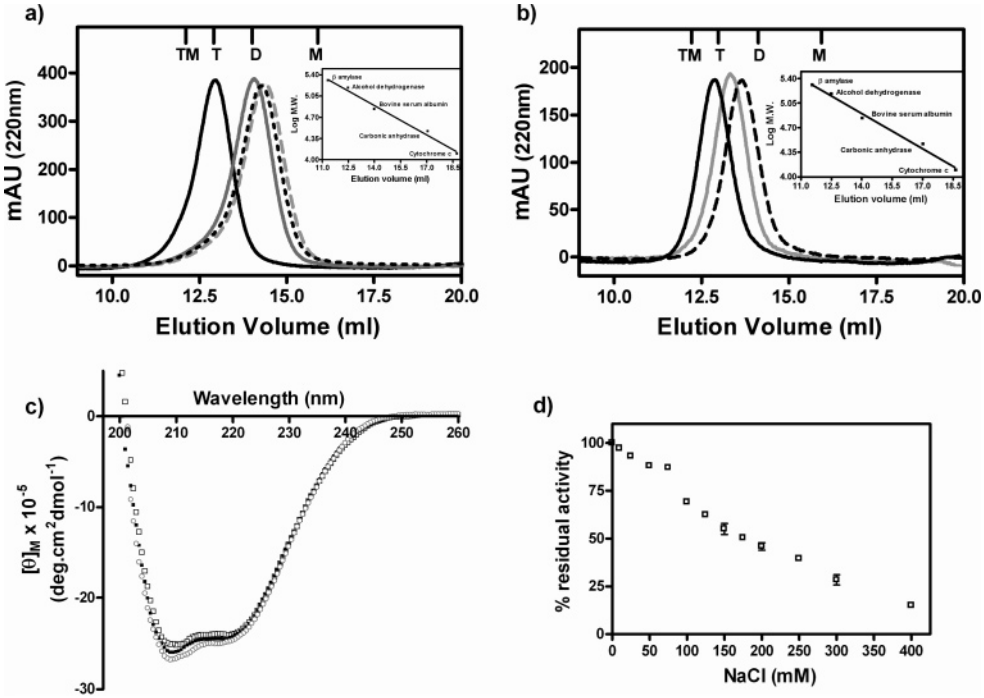

FIGURE 3: Effect of NaCl and substrates on the structure and function of MjAdSS. Elution profile of MjAdSS on an analytical Superdex 200 column in the presence of (a) different NaCl concentrations (black solid line, 0 mM NaCl; gray solid line, 50 mM NaCl; black dashed line, 100 mM NaCl, and gray dashed line, 1.2 M NaCl) and (b) substrates (black solid line, protein alone; black dashed line, protein with 2 mM magnesium acetate, and gray solid line, protein with magnesium acetate, IMP, and GTP. The inset shows the calibration curve of log MW of standard proteins vs elution volume. M, monomer; D, dimer; T, trimer; TM, tetramer. M, D, T, and TM indicated on top of the panels correspond to calculated elution volumes for the monomer, dimer, trimer, and tetramer of MjAdSS. (c) Far-UV CD spectra of MjAdSS in 20 mM Tris HCl at pH 7.4 and 0 mM NaCl (□), 300 mM NaCl (■), and 1.2 M NaCl (○). (d) Effect of NaCl on MjAdSS activity. Activity in the absence of NaCl was taken as 100%.

mechanism of MjAdSS, initial velocity measurements were made following the method developed by Fromm (*18*, *34*). IMP, GTP, and Asp were varied in separate experiments, where the concentration of the other two substrates was varied simultaneously in a fixed ratio around their respective K_m values. The results are summarized in Figure 4 (a−c). The absence of parallel pattern in the plots indicates that no product is released before the binding of all three substrates, thereby ruling out a ping−pong mechanism. Convergence of lines in each of the plots in Figure 4 is indicative of a sequential mechanism. The lines in double reciprocal plots of initial velocity versus IMP or GTP concentration converged in the second quadrant, whereas lines in plots of $1/v$ versus 1/[Asp] intersected on the *y*-axis. A similar intersection pattern with variable aspartate was obtained in two independent experiments using enzyme from two different batches of purification. The crossover point of $1/v$ versus 1/[Asp] plots continued to be on the *y*-axis when either IMP or GTP were held at constant saturating concentration (Figure 4f). This intersection pattern obtained with aspartate as the variable substrate rules out a number of kinetic models viz. a rapid equilibrium completely random mechanism, steady-state completely ordered mechanism, a completely ordered mechanism where E-EA or EA-EAB forms are in rapid equilibrium, a random AB mechanism where E-EA and E-EB forms are in rapid equilibrium, a rapid equilibrium random BC or random AC mechanism, and a random BC model where EA-EAC and EA-EAB (±EABC) forms are in rapid equilibrium from consideration, as these models would require a family of lines intersecting to the left of the $1/v$ axis with all three variable substrates. Therefore, these results are indicative of either (i) a completely ordered mechanism where all enzyme forms or E-EA-EAB are in rapid equilibrium or (ii) random AB ordered C kinetic mechanism where all enzyme forms or E, EA, EB, and EAB are in rapid equilibrium, and EABC is in steady-state (*35* (pp 699−749)). Here, A, B, and C indicate IMP, GTP, and aspartate, respectively. The equations for rapid equilibrium completely ordered (eq 3) and rapid equilibrium random AB ordered C (eq 4) terreactant systems are given below. The equation for partial rapid equilibrium reaction where E, EA, EB, and EAB are in rapid equilibrium and EAB + C → EABC and its interconversion is in steady-state has the same form as that for the full rapid equilibrium random AB ordered C system (eq 4) (*35* (pp 699−749)).

$$v/V_{max} = [A][B][C]/(K_A K_B K_C + K_B K_C [A] + K_C [A][B] + [A][B][C]) \quad (3)$$

$$v/V_{max} = [A][B][C]/(\alpha K_A K_B K_C + \alpha K_B K_C [A] + \alpha K_A K_C [B] + K_C [A][B] + [A][B][C]) \quad (4)$$

In the above equations, A, B, and C are as described earlier, v is the initial velocity, and V_{max} is the maximum velocity. K_A, K_B, and K_C in eq 3 are the Michaelis constants for A, B, and C, respectively. In eq 4, K_A and K_B denote the dissociation constants for substrates A and B, respectively, whereas, αK_A, αK_B, and K_C are Michaelis constants for the three substrates.

To further distinguish between the above two models, the initial velocity measurements were made using the method

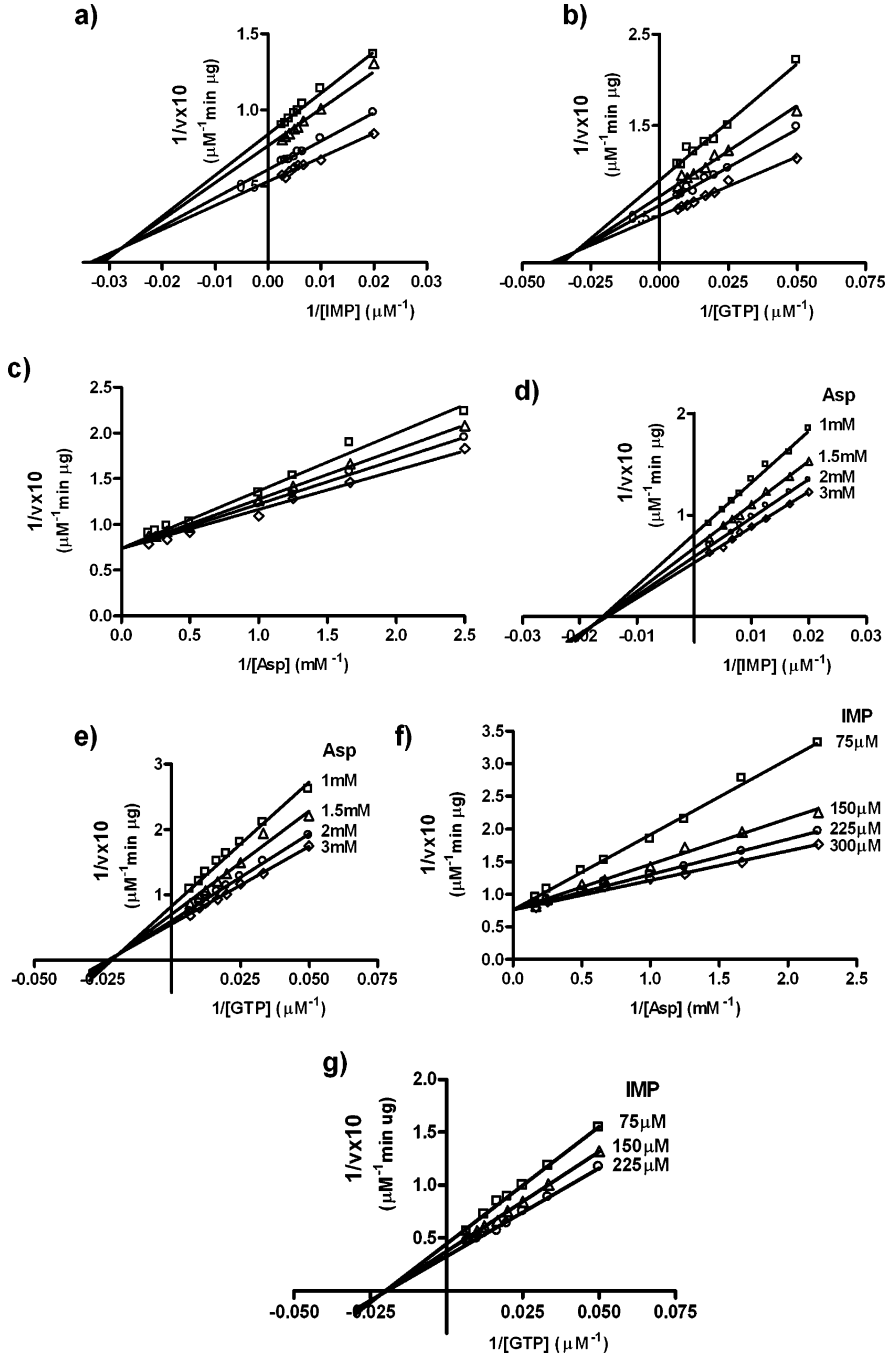

FIGURE 4: Plots of reciprocal of initial velocity (v) with respect to the reciprocal of substrate concentration. a−c represent plots from initial velocity measurements where two substrates were varied in a fixed ratio. (a) IMP concentration was varied from 50 to 375 μM and the respective concentrations of aspartate and GTP were 1.2 mM and 65 μM (□); 1.65 mM and 90 μM (△); 2.4 mM and 133 μM (○); and 4.0 mM and 220 μM (◇). (b) GTP concentration was varied from 20 to 150 μM. The respective concentrations of aspartate and IMP were 1.2 mM and 100 μM (□); 1.65 mM and 137.5 μM (△); 2.4 mM and 200 μM (○); and 4.0 mM and 335 μM (◇). (c) Aspartate concentration was varied from 0.45 mM to 5 mM. The respective concentrations of IMP and GTP were 80 and 40 μM (□); 120 and 60 μM (△); 170 and 85 μM (○); and 320 and 160 μM (◇). d−g are plots from initial velocity measurements where one substrate was held at saturating concentration. (d) IMP concentration was varied from 50 to 375 μM, and GTP was held constant at 250 μM. The concentration of aspartate is indicated against each line. (e) GTP concentration was varied from 20 to 150 μM, and IMP was held constant at 500 μM. The fixed concentration of aspartate is indicated against each line. (f) Aspartate was varied from 0.45 mM to 6.0 mM, and GTP was held constant at 250 μM. The concentration of IMP is indicated against each line. (g) GTP was varied from 20 to 150 μM, and aspartate was fixed at 10 mM. The fixed concentration of IMP is indicated against each line.

proposed by Frieden, where one substrate was held constant and the other two were varied (*36*) (Figure 4d−g). A family of lines intersecting in the third quadrant was obtained when aspartate was held at saturating concentration, and GTP was varied at different fixed concentrations of IMP (Figure 4g). This pattern is clearly indicative of a random AB ordered C mechanism. For a completely ordered mechanism, the lines would intersect on the *y*-axis (*35* (pp 273−345)). When IMP or GTP was held at saturating concentration with aspartate as the fixed variable, the family of lines again converged close to the horizontal axis in the second and third quadrant, respectively (Figure 4d and e). Under these conditions, the

Table 2: Rapid Equilibrium Random AB Steady-state Ordered C Kinetic Model for MjAdSS[a]

equilibrium	constant	value from fits
	V_{max}	$26.0 \pm 2.0\ \mu M\ min^{-1}\ \mu g^{-1}$
		$26.0 \pm 0.9\ \mu M\ min^{-1}\ \mu g^{-1}$
		mean $= 26.0\ \mu M\ min^{-1}\ \mu g^{-1}$
	k_{cat}[b]	$5.0\ s^{-1}$
EA = E + A	K_A	$64.4 \pm 12.3\ \mu M$
EB = E + B	K_B	$58.03 \pm 17.4\ \mu M$
EAB = EB + A	αK_A	$70.2 \pm 7.1\ \mu M$
EAB = EA + B	αK_B	$44.9 \pm 8.6\ \mu M$
EABC = EAB + C	K_C	1.0 ± 0.2 mM
		1.0 ± 0.1 mM
		mean = 1.0 mM
	$\alpha = \alpha K_A/K_A$	1.1
	$\alpha = \alpha K_B/K_B$	0.8
		mean = 0.95

[a] The symbol E represents MjAdSS; A, B, and C represent IMP, GTP, and aspartate, respectively. The kinetic constants are defined explicitly with reference to Scheme 1. [b] $k_{cat} = V_{max}/[E]_T$

system can be treated as a bireactant system. The data were fit to eqs 5 and 6, which denote a rapid equilibrium ordered and steady-state ordered bisubstrate reaction, respectively.

$$v/V_{max} = [A][C]/(K_A K_C + K_C\,[A] + [A][C]) \text{ for variable A, at saturating B}$$

$$v/V_{max} = [B][C]/(K_B K_C + K_C\,[B] + [B][C]) \text{ for variable B, at saturating A} \quad (5)$$

$$v/V_{max} = [A][C]/(K_A K_C + K_C\,[A] + \alpha K_A\,[C] + [A][C]) \text{ for variable A, at saturating B}$$

$$v/V_{max} = [B][C]/(K_B K_C + K_C\,[B] + \alpha K_B\,[C] + [B][C]) \text{ for variable B, at saturating A} \quad (6)$$

The constants K_A, K_B, K_C, αK_A and αK_B in eqs 5 and 6 are as defined earlier. The fit to eq 5 yielded inferior results and negative values for at least one constant. The data fitted well to eq 6, the results of which are summarized in Table 2. The k_{cat} values obtained from fits agree well with those reported in Table 1. The K_C value is close to that of K_m for aspartate, and the αK_A and αK_B values for IMP and GTP agree with their K_m values in Table 1. An α value close to 1 indicates that IMP and GTP bind independently to the enzyme. Steady-state ordered binding of aspartate is also supported by the intersection of lines in the second and third quadrant in plots of $1/v$ versus 1/[GTP] and 1/[IMP], respectively, at different fixed concentrations of aspartate and a saturating concentration of the third substrate (Figure 4d and e). Taken together, the initial velocity data indicate that IMP and GTP bind randomly to the enzyme and that the binding of aspartate to the E−IMP−GTP complex is steady-state ordered. Thus, MjAdSS exhibits rapid equilibrium random AB steady-state ordered C kinetic mechanism.

Product Inhibition Studies. Products that are structural mimics of the substrates when used as inhibitors in initial velocity measurements serve to confirm the order of substrate binding in multi-substrate reactions. The effect of competitive inhibitors is measured by plots of $1/v$ versus 1/[varied ligand] at different fixed concentrations of the inhibitor and constant unsaturating concentrations of the other two coligands (*37*, *38*). In a rapid equilibrium random AB steady-state ordered C kinetic mechanism, a competitive inhibitor of A or B would show noncompetitive inhibition with the other two substrates and competitive inhibitor of C would be an uncompetitive inhibitor of A and B (*35* (pp 699−749)). The products of the reaction catalyzed by AdSS are sAMP, GDP, and Pi. Pi, not being a specific mimic of any of the three substrates, does not serve to confirm the order of substrate binding. Hadacidin (*N*-formyl *N*-hydroxyglycine), a secondary metabolite from *Penicillium frequentans* (*39*), is a potent inhibitor of AdSS, competing for the aspartate binding pocket (*40*−*45*). Hence, inhibition patterns with the products sAMP, GDP, and the aspartate mimic, hadacidin were examined for MjAdSS. The double reciprocal plots of the initial velocity in the presence of the inhibitors are summarized in Figure S1 in the Supporting Information. The data were analyzed by fits to the kinetic models for competitive, noncompetitive, and uncompetitive inhibition (eqs 7−9).

$$v = V_{max}\,[S]/\{K_m\,(1+I/K_i) + [S]\} \text{ competitive inhibition} \quad (7)$$

$$v = V_{max}\,[S]/\{K_m\,(1+I/K_i) + [S]\,(1+I/K_i)\} \text{ noncompetitive inhibition} \quad (8)$$

$$v = V_{max}\,[S]/\{K_m + [S]\,(1+I/K_i)\} \text{ uncompetitive inhibition} \quad (9)$$

where v and V_{max} are initial and maximum velocities, respectively, I is inhibitor concentration, S is the variable substrate concentration, K_i is the inhibition constant, and K_m is the Michaelis constant for the variable substrate. The best fits were selected on the basis of F test and *P* values. Table 3 lists the K_i values and the inhibition pattern obtained from a nonlinear regression fit of the data to appropriate models.

sAMP, a competitive inhibitor of IMP was a noncompetitive inhibitor of GTP and aspartate (Table 3). GDP, which was a competitive inhibitor of GTP, showed noncompetitive inhibition with IMP and aspartate (Table 3). This pattern of inhibition supports the random binding of IMP and GTP to the enzyme. However, hadacidin, a competitive inhibitor of aspartate, showed uncompetitive inhibition with IMP and GTP (Table 3). The family of parallel lines indicate that both V_{max} and K_m are modulated with IMP and GTP as the variable substrates. Similar results were obtained when the two fixed substrates (either IMP and aspartate or GTP and aspartate) were held at saturating concentrations with respect to their K_m (data not shown). This shows that hadacidin, and hence aspartate binding is conditional to the catalytic pocket being occupied by both IMP and GTP. This further supports the random AB ordered C substrate binding seen from initial velocity measurements.

Of the three products generated in the reaction catalyzed by AdSS, Pi does not inhibit *P. falciparum* AdSS and is a poor inhibitor of rat skeletal muscle AdSS with 59% inhibition seen at 20 mM phosphate (*46*). However, Pi was found to be a potent inhibitor of MjAdSS with the concentration dependence of Pi on enzyme activity showing a biphasic trend (Figure 5a). Intersection patterns on Dixon plots were characteristic of competitive inhibition with IMP and noncompetitive inhibition with respect to GTP (Figure

Table 3: Summary of MjAdSS Inhibition Kinetics Using Products and Substrate Analogues[a]

	inhibitor						
substrate	sAMP[b]	GDP[b]	hadacidin[b]	AMP[b]	GMP[b]	F16BP[c]	phosphate[c]
IMP	competitive $K_{iapp} = 9.4 \pm 0.9$	noncompetitive $K_{iapp} = 82.2 \pm 3.9$	uncompetitive $K_{iapp} = 26.4 \pm 1.2$	competitive $K_{iapp} = 58.2 \pm 6.7$	noncompetitive $K_{iapp} = 110.6 \pm 2.1$	competitive $K_{iapp} = 1.5 \pm 0.1$	competitive $K_{iapp} = 1.9 \pm 0.2$
GTP	noncompetitive $K_{iapp} = 42.9 \pm 2.4$	competitive $K_{iapp} = 7.0 \pm 0.8$	uncompetitive $K_{iapp} = 26.9 \pm 1.4$	noncompetitive $K_{iapp} = 402.6 \pm 11.3$	competitive $K_{iapp} = 13.7 \pm 1.4$	noncompetitive $K_{iapp} = 4.8 \pm 0.2$	noncompetitive $K_{iapp} = 8.3 \pm 0.4$
aspartate	noncompetitive $K_{iapp} = 42.6 \pm 2.1$	noncompetitive $K_{iapp} = 82.1 \pm 4.2$	competitive $K_{iapp} = 10.5 \pm 1.0$	noncompetitive $K_{iapp} = 324.0 \pm 20.1$	noncompetitive $K_{iapp} = 120.8 \pm 3.3$	ND	ND

[a] K_{iapp} is the apparent inhibition constant. [b] K_{iapp} values are in μM. [c] K_{iapp} values are in mM; ND, not determined.

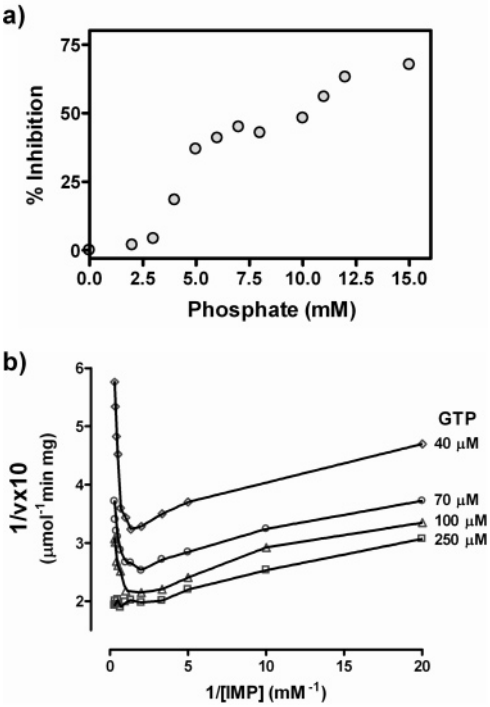

FIGURE 5: Regulation of MjAdSS activity by (a) Pi and (b) IMP. (a) Effect of increasing Pi concentration on MjAdSS activity. Activity in the absence of Pi was taken as 0% inhibition. IMP, GTP, and aspartate concentrations were held constant at 500 μM, 250 μM, and 10 mM, respectively. (b) Double reciprocal plot of initial velocity and IMP concentration at different fixed concentrations of GTP. Aspartate concentration was held constant at 10 mM.

S2 Ia, b in the Supporting Information). To determine the K_i values, the data were fitted to eqs 10 and 11.

$$1/v = \{K_m/(V_{max}[S]K_i)\}[I] + \{1/V_{max}(1 + K_m/[S]\} \text{ for competitive inhibition} \quad (10)$$

$$1/v = \{(1+K_m/[S])/V_{max}K_i\}[I] + \{1/V_{max}(1 + K_m/[S]\} \text{ for noncompetitive inhibition} \quad (11)$$

The apparent K_i values for IMP and GTP were determined to be 1.9 ± 0.2 mM and 8.3 ± 0.4 mM, respectively. Among the K_i values for the products, that for Pi is the highest followed by GDP and sAMP having similar but significantly lower values (Table 3). This indicates that Pi is liberated first from the enzyme followed by sAMP and GDP adopting a random order of release from MjAdSS. The overall kinetic mechanism as deduced from initial velocity and product inhibition studies for MjAdSS is shown in Scheme 1.

Scheme 1: Proposed Kinetic Mechanism for *M. jannaschii* Adenylosuccinate Synthetase Catalyzed Reaction[a]

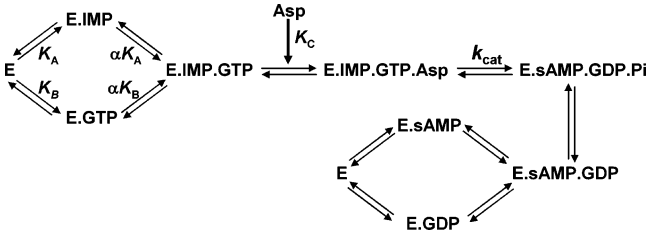

[a] The enzyme follows the rapid equilibrium random AB steady-state ordered C kinetic mechanism, where A, B and C represent IMP, GTP, and aspartate, respectively.

Modulation of MjAdSS Activity by Metabolites. AdSS is a branch point enzyme with its substrate IMP also being utilized by inosine monophosphate dehydrogenase, the enzyme that catalyzes the first step in the biosynthesis of GMP. Hence, the regulation of AdSS activity by various metabolites becomes an important feature in the context of cellular biochemistry. Metabolites that are known to modulate AdSS activity are GDP, sAMP, GMP, AMP, IMP, and F16BP (*47*). Table 3 provides a summary of the K_i values of these inhibitors for MjAdSS.

High concentrations of IMP (>1 mM) at subsaturating concentrations of GTP inhibited MjAdSS, and this inhibition was relieved at high GTP concentration. The $1/v$ versus 1/[IMP] curves at different fixed concentrations of GTP showed parabolic behavior characteristic for substrate inhibition where the AdSS−$(IMP)_2$ dead end complex is formed (Figure 5b). Secondary plot of $slope_{1/GTP}$ versus 1/[IMP] was also parabolic (data not shown), reinforcing the AdSS−$(IMP)_2$ dead end complex formation (*48*, *32* (pp 191−207)). Inhibition of MjAdSS by AMP, like sAMP, was competitive with respect to IMP and noncompetitive with GTP and aspartate. However, unlike sAMP, AMP was a weak inhibitor with a K_i value of 58.2 μM. Like that of GDP, GMP inhibition was competitive with respect to GTP and noncompetitive with IMP and aspartate (Table 3). The inhibition patterns seen with AMP and GMP also support the random binding of the substrates IMP and GTP to MjAdSS.

The glycolyitc intermediate, fructose 1,6 bisphosphate (F16BP), is a known modulator of AdSS activity (*12*, *43*, *44*, *49*). Inhibition patterns from Dixon plots indicated competitive inhibition with respect to IMP and noncompetitive inhibition with GTP (Figure S2 IIa, b in the Supporting Information). The data were fit to eqs 10 and 11 to determine the K_i value. Apparent K_i values of 1.5 ± 0.1 mM and 4.8 ± 0.2 mM were obtained for IMP and GTP, respectively, which are significantly higher than those reported for mouse acidic AdSS (*12*).

DISCUSSION

Adenylosuccinate synthetase from the thermophilic archaea *M. jannaschii* is 90−120 amino acids shorter than the biochemically and structurally well characterized counterparts from the mesophiles, *E. coli*, mouse, and *P. falciparum*. Our studies toward the characterization of a thermophilic AdSS highlight certain unique kinetic and regulatory features of this enzyme. IMP and GTP K_m values for MjAdSS are higher than those reported for other AdSS in literature (Table 1), while the aspartate K_m value is similar to that for the mouse acidic isozyme. The catalytic efficiency of MjAdSS at 70 °C is comparable to mouse acidic AdSS at ambient temperature, whereas at 25 °C, *P. falciparum* and *E. coli* AdSS exhibit lower k_{cat} values of 1.1 and 1.4 s^{-1}, respectively (*6*, *20*).

Crystallography and mutation analysis have shown that AdSS function as homodimers with both subunits contributing to the two active sites. The side chain of Arg 143 (*E. coli* numbering) from one subunit penetrates the active site cleft of the symmetry related subunit and hydrogen bonds the 5′ phosphate group of IMP. A complete active site thus requires structural elements from both subunits of the dimer (*5*, *6*, *27*). *E. coli*, *P. falciparum*, and yeast AdSS exhibit monomer−dimer equilibrium in solution, while mouse acidic and basic isozymes are predominantly dimers (*6*, *12*, *45*, *50*). It is interesting to note that the *M. jannaschii* enzyme in solution exhibits dimer−tetramer equilibrium, and this subunit association was found to be essential for enzyme activity (Figure 3). The extremely tight MjAdSS dimer may be a prerequisite for the thermostability of the enzyme.

Variation in the kinetic mechanism of AdSS from different species has been reported. Initial velocity kinetics and product inhibition studies have established a rapid equilibrium random sequential mechanism for *E. coli* AdSS (*18*). Similar studies with human, *Schizosaccharomyces pombe* and *Dictyostelium discoideum* AdSS indicate a random sequential mechanism for the forward reaction (*51*−*53*). AdSS catalyzes a reversible reaction, and the elucidation of steady-state kinetic mechanism of *Azotobacter vinelandii* AdSS in both directions highlighted random sequential binding for forward and reverse reactions (*43*). While similar results were obtained for rat muscle AdSS by equilibrium isotope exchange, these studies highlighted a preferred binding path in the forward reaction with the quaternary complex being formed by aspartate binding to the E−IMP−GTP complex (*19*). This indicates that substrate induced conformational changes in the enzyme may be important in achieving a proper disposition of the active site for catalysis. In contrast, an ordered binding of substrates to the *P. falciparum* enzyme (*20*) was observed by product inhibition studies, with IMP binding first followed by GTP and then aspartate. Initial velocity kinetics and product inhibition studies with MjAdSS are consistent with rapid equilibrium random binding of IMP and GTP followed by steady-state ordered binding of aspartate to the E−IMP−GTP complex. This work is the second report of an enzyme exhibiting random AB ordered C kinetic mechanism with the first being that of guanylate cyclase (*54*).

Adenylosuccinate synthetase is an integral part of both de novo and salvage pathways for purine nucleotide biosynthesis, both of which proceed through the common intermediate, IMP. This is the first enzyme that commits IMP to the formation of AMP, and hence, it is implicated in maintaining AMP/GMP ratios in the cell (*47*). Studies in literature have highlighted different aspects of regulation of the enzyme by components of the purine biosynthesis pathway and intermediates from the glycolytic pathway (*47*). Vertebrates have acidic and basic isozymes of AdSS, which have been implicated in de novo biosynthesis of AMP and purine nucleotide cycle, respectively. These isozymes differ in kinetic properties and response to inhibitors, thereby indicating different modes of regulation of the two enzymes. Like the mouse acidic isozyme and *P. falciparum* AdSS (*12*, *20*), MjAdSS shows inhibition by IMP when GTP is limiting. In contrast, mouse basic isozyme is inhibited by high concentrations of IMP even at saturating concentrations of GTP (*12*). The substrate inhibition pattern of MjAdSS is consistent with E-$(IMP)_2$ dead end complex formation, indicating IMP binding to GTP site at subsaturating concentrations of GTP. This alternate binding mode of IMP is also evident in the crystal structure of an IMP complex of mouse basic AdSS (*55*). Products of the reaction, sAMP, GDP, and Pi, were also found to be effective regulators of enzyme activity. Studies with rabbit skeletal muscle AdSS suggest noncompetitive phosphate inhibition with all three substrates, albeit with high K_i values (*56*). Noncompetitive Pi inhibition with respect to GTP has been reported for *E. coli* AdSS. However, a significantly high concentration of Pi (>10 mM) was required for the detection of inhibition (*18*). The biphasic inhibition curve at varying phosphate concentration implies two binding sites on MjAdSS, with one being the IMP binding site. The identity of the second site could not be established from these studies.

The acidic and basic isozymes of mammalian AdSS have been assigned to separate metabolic pathways based on susceptibility to inhibition by nucleotides and F16BP. The mouse basic isozyme exhibits greater sensitivity to inhibition by F16BP with the K_i value being 8-fold lower than that for the acidic isozyme (*12*). Noncompetitive inhibition of F16BP with respect to all substrates has been reported in rat skeletal muscle AdSS and mouse isozymes (*12*, *49*). This inhibition pattern invokes an inhibitory site distinct from the active site. However, a preliminary crystallographic study by Borza et al. suggests that F16BP occupies the 6-phosphoryl-IMP binding site. Thus, these studies indicate that at low concentrations of IMP, F16BP competes for the IMP binding site, but when the concentration of substrate is high, it binds to a site, still unidentified (*12*). This feature is also reflected in MjAdSS, where a competitive inhibition pattern with respect to IMP was seen when the substrates were nonsaturating. In contrast, *P. falciparum* AdSS is the only enzyme that exhibits activation with F16BP when assays are initiated with aspartate (*20*).

These results highlight that in different organisms and different tissue types, modulation of AdSS activity by certain ligands is conserved, while other metabolites exhibit marked variation. These differences in turn reflect dissimilarities in metabolic flux and in modes of regulation across organisms.

Structural Implications for the Observed Kinetic Mechanism of MjAdSS. An examination of the NCBI database shows that short AdSS sequences do not segregate solely to thermophilic organisms. Certain mesophilic organisms also have short AdSS sequences, thereby indicating that the

deletion of segments A and B may not necessarily be associated with thermal stability. Apart from the deletion of segments A and B, the rest of the sequence shows high conservation across long and short AdSS (Figure 1a). The structure of *Pyrococcus horikoshii* adenylosuccinate synthetase (PhAdSS), also a short AdSS, has been recently solved by the RIKEN Structural Genomics/Proteomics Initiative (RSGI) (PDB ID: 2D7U, Xie, Y., Kishishita, S., Muarayama, K., Shirouzu, M., and Yokoyama, S., Crystal structure of hypothetical adenylosuccinate synthetase, PH0438 from *Pyrococcus horioshii* OT3). The 68% sequence identity between the AdSS sequences of *M. jannaschii* and *P. horikoshii* permits structure−function correlations to be made using the available structure of Pyrococcus AdSS. The deletions A and B fall in subdomains II and IV, respectively (*15*). Though the deleted segments in MjAdSS form a part of subdomains that are associated with ligand binding and interface contacts, the residues within these segments do not contribute significantly to either ligand or intersubunit contacts. The superposition of the *E. coli* and *Pyrococcus* structures shows that the two ends of the deleted segments get connected by loops. Interestingly, no gross structural reorganization is evident in the core of the protein as a consequence of the deletions.

A comparison of various liganded and unliganded structures of AdSS reveals that there are 5 loops that respond to substrate binding, namely, the Switch loop, IMP loop, GTP loop, Asp loop, and Val loop (*14*, *27*). IMP bound structures of *E. coli* and mouse AdSS indicate that IMP binding is sufficient to organize all loops except the Asp loop that responds to hadacidin binding (*31*, *57*). The structure of the unliganded *P. horikoshii* AdSS (PDB ID: 2D7U) has four loops in the closed conformation with the IMP loop not mapped. This is the first structure of AdSS with a loop-closed conformation in the absence of ligands. Absence of contacts between the loop residues shows that such interactions cannot contribute to the stability of the closed state. The loop-closed conformation in the *Pyrococcus* AdSS structure may be stabilized because of energy contributions from the interactions of loop residues with amino acids in other segments of the protein.

A comparison of the fully liganded PfAdSS structure with mouse and *E. coli* structures highlights differences that could be contributing to the ordered substrate binding in PfAdSS. Hydrogen bonding of Ser 57 and Asp 60 in the Switch loop with Asn 429 in GTP loop results in inward movement of the Switch loop into the ligand binding pocket. As a result, nonconserved Lys 62 in the Switch loop hydrogen bonds with ribose hydroxyls of GDP (*15*). These residues are not conserved in mouse, *E. coli* and *Methanococcus* AdSS, which show random binding of IMP and GTP. In the liganded PfAdSS structure, GDP hydrogen bonds with the side chain hydroxyl of Thr 307 on the Asp loop, indicating that GTP binding brings about loop movements that prepare the cavity for aspartate binding (*15*). Thr 307, not conserved in mouse and *E. coli* AdSS while being conserved in MjAdSS, could possibly dictate ordered binding of aspartate in a manner analogous to that observed in the parasite enzyme. The orientation of the two catalytic residues Asp 13 and His 43 in the unliganded *Pyrococcus* structure is comparable to liganded crystal structures of *E. coli*, mouse, and *P. falciparum* AdSS, whereas a comparison with unliganded mouse or *E. coli* structures shows good overlap of Asp 13, but His 43 is flipped by 180°. Therefore, this indicates that the *Pyrococcus* enzyme is fully poised for catalysis and that the loop movements are driven even in the absence of ligands. The availability of the liganded structure of MjAdSS should provide the structural implication for the observed random AB ordered C kinetic mechanism.

ACKNOWLEDGMENT

We thank Professor Rama Govindarajan, Engineering Mechanics Unit, JNCASR, and Professor S. Balasubramanian, Chemistry and Physics of Materials Unit, JNCASR for useful discussions during the mathematical analysis of kinetic data. We thank the Developmental Therapeutics Program, National Cancer Institute, NIH, Bethesda, MD, for providing hadacidin.

SUPPORTING INFORMATION AVAILABLE

Figures showing Lineweaver−Burk plots for the inhibition of MjAdSS by products and substrate analogues (Figure S1) and Dixon analysis of the inhibition of MjAdSS by Pi and F16BP (Figure S2). This material is available free of charge via the Internet at http://pubs.acs.org.

REFERENCES

1. Lieberman, I. (1956) Enzymatic synthesis of adenosine-5′-phosphate from inosine-5′-phosphate, *J. Biol. Chem. 223*, 327−339.
2. Fromm, H. J. (1958) On the equilibrium and mechanism of adenylosuccinic acid synthesis, *Biochim. Biophys. Acta 29*, 255−262.
3. Bass, M. B., Fromm, H. J., and Rudolph, F. B. (1984) The mechanism of the adenylosuccinate synthetase reaction as studied by positional isotope exchange, *J. Biol. Chem. 259*, 12330−12333.
4. Poland, B. W., Bruns, C., Fromm, H. J., and Honzatko, R. B. (1997) Entrapment of 6-thiophosphoryl-IMP in the active site of crystalline adenylosuccinate synthetase from *Escherichia coli*, *J. Biol. Chem. 272*, 15200−15205.
5. Kang, C., Kim, S., and Fromm, H. J. (1996) Subunit complementation of *Escherichia coli* adenylosuccinate synthetase, *J. Biol. Chem. 271*, 29722−29728.
6. Wang, W., Gorrell, A., Honzatko, R. B., and Fromm, H. J. (1997) A study of *Escherichia coli* adenylosuccinate synthetase association states and the interface residues of the homodimer, *J. Biol. Chem. 272*, 7078−7084.
7. Honzatko, R. B., Stayton, M. M., and Fromm, H. J. (1999) Adenylosuccinate synthetase: recent developments, *Adv. Enzymol. Relat. Areas Mol. Biol. 73*, 57−102.
8. Fonne-Pfister, R., Chemla, P., Ward, E., Girardet, M., Kreuz, K. E., Honzatko, R. B., Fromm, H. J., Schar, H. P., Grutter, M. G., and Cowan-Jacob, S. W. (1996) The mode of action and the structure of a herbicide in complex with its target: binding of activated hydantocidin to the feedback regulation site of adenylosuccinate synthetase, *Proc. Natl. Acad. Sci. U.S.A. 93*, 9431−9436.
9. Prade, L., Cowan-Jacob, S. W., Chemla, P., Potter, S., Ward, E., and Fonne-Pfister, R. (2000) Structures of adenylosuccinate synthetase from *Triticum aestivum* and *Arabidopsis thaliana*, *J. Mol. Biol. 296*, 569−577.
10. Spector, T., Jones, T. E., and Elion, G. B. (1979) Specificity of adenylosuccinate synthetase and adenylosuccinate lyase from *Leishmania donovani*. Selective amination of an antiprotozoal agent, *J. Biol. Chem. 254*, 8422−8426.
11. Matsuda, Y., Ogawa, H., Fukutome, S., Shiraki, H., and Nakagawa, H. (1977) Adenylosuccinate synthetase in rat liver: the existence of two types and their regulatory roles, *Biochem. Biophys. Res. Commun. 78*, 766−771.
12. Borza, T., Iancu, C. V., Pike, E., Honzatko, R. B., and Fromm, H. J. (2003) Variations in the response of mouse isozymes of adenylosuccinate synthetase to inhibitors of physiological relevance, *J. Biol. Chem. 278*, 6673−6679.

13. Poland, B. W., Silva, M. M., Serra, M. A., Cho, Y., Kim, K. H., Harris, E. M., and Honzatko, R. B. (1993) Crystal structure of adenylosuccinate synthetase from *Escherichia coli*. Evidence for convergent evolution of GTP-binding domains, *J. Biol. Chem. 268*, 25334−25342.
14. Iancu, C. V., Borza, T., Choe, J. Y., Fromm, H. J., and Honzatko, R. B. (2001) Recombinant mouse muscle adenylosuccinate synthetase: overexpression, kinetics, and crystal structure, *J. Biol. Chem. 276*, 42146−42152.
15. Eaazhisai, K., Jayalakshmi, R., Gayathri, P., Anand, R. P., Sumathy, K., Balaram, H., and Murthy, M. R. (2004) Crystal structure of fully ligated adenylosuccinate synthetase from *Plasmodium falciparum*, *J. Mol. Biol. 335*, 1251−1264.
16. Bouyoub, A., Barbier, G., Forterre, P., and Labedan, B. (1996) The adenylosuccinate synthetase from the hyperthermophilic archaeon Pyrococcus species displays unusual structural features, *J. Mol. Biol. 261*, 144−154.
17. Cann, I. K., Kanai, S., Toh, H., and Ishino, Y. (1998) Adenylosuccinate synthetase genes: molecular cloning and phylogenetic analysis of a highly conserved archaeal gene, *Syst. Appl. Microbiol. 21*, 478−486.
18. Rudolph, F. B., and Fromm, H. J. (1969) Initial rate studies of adenylosuccinate synthetase with product and competitive inhibitors, *J. Biol. Chem. 244*, 3832−3839.
19. Cooper, B. F., Fromm, H. J., and Rudolph, F. B. (1986) Isotope exchange at equilibrium studies with rat muscle adenylosuccinate synthetase, *Biochemistry 25*, 7323−7327.
20. Raman, J., Mehrotra, S., Anand, R. P., and Balaram, H. (2004) Unique kinetic mechanism of *Plasmodium falciparum* adenylosuccinate synthetase, *Mol. Biochem. Parasitol. 138*, 1−8.
21. Laemmli, U. K. (1970) Cleavage of structural proteins during the assembly of the head of bacteriophage T4, *Nature 227*, 680−685.
22. Bradford, M. M. (1976) A rapid and sensitive method for the quantitation of microgram quantities of protein utilizing the principle of protein-dye binding, *Anal. Biochem. 72*, 248−254.
23. Carey, N. H., and Mandel, H. G. (1961) Studies on the inhibition of growth of *Bacillus cereus* by 6-mercaptopurine, *J. Biol. Chem. 236*, 520−524.
24. Kang, C., and Fromm, H. J. (1995) Identification of an essential second metal ion in the reaction mechanism of *Escherichia coli* adenylosuccinate synthetase, *J. Biol. Chem. 270*, 15539−15544.
25. Tipton, K. F., and Dixon, H. B. (1979) Effect of pH on enzymes, *Methods Enzymol. 63*, 183−234.
26. Dixon, M. (1953) The determination of enzyme inhibitor constants, *Biochem. J. 55*, 170−171.
27. Poland, B. W., Fromm, H. J., and Honzatko, R. B. (1996) Crystal structures of adenylosuccinate synthetase from *Escherichia coli* complexed with GDP, IMP hadacidin, NO^{3-}, and Mg^{2+}, *J. Mol. Biol. 264*, 1013−1027.
28. Kang, C., Sun, N., Poland, B. W., Gorrell, A., Honzatko, R. B., and Fromm, H. J. (1997) Residues essential for catalysis and stability of the active site of *Escherichia coli* adenylosuccinate synthetase as revealed by directed mutation and kinetics, *J. Biol. Chem. 272*, 11881−11885.
29. Choe, J. Y., Poland, B. W., Fromm, H. J., and Honzatko, R. B. (1999) Mechanistic implications from crystalline complexes of wild-type and mutant adenylosuccinate synthetases from *Escherichia coli*, *Biochemistry 38*, 6953−6961.
30. Poland, B. W., Lee, S. F., Subramanian, M. V., Siehl, D. L., Anderson, R. J., Fromm, H. J., and Honzatko, R. B. (1996) Refined crystal structure of adenylosuccinate synthetase from *Escherichia coli* complexed with hydantocidin 5′-phosphate, GDP, $HPO4^{2-}$, Mg^{2+}, and hadacidin, *Biochemistry 35*, 15753−15759.
31. Iancu, C. V., Borza, T., Fromm, H. J., and Honzatko, R. B. (2002) IMP, GTP, and 6-phosphoryl-IMP complexes of recombinant mouse muscle adenylosuccinate synthetase, *J. Biol. Chem. 277*, 26779−26787.
32. Leskovac, V. (2003) *Comprehensive Enzyme Kinetics*, pp 139−170, 191−207, 209−241, Kulwer Academic/Plenum Publishers, New York.
33. Bridger, W. A., and Cohen, L. H. (1968) The kinetics of adenylosuccinate lyase. *J. Biol. Chem. 243*, 644−650.
34. Rudolph, F. B., and Fromm, H. J. (1979) Plotting methods for analyzing enzyme rate data, *Methods Enzymol. 63*, 138−159.
35. Segel, I. H. (1975) *Enzyme Kinetics. Behaviour and Analysis of Rapid Equilibrium and Steady-state Enzyme Systems*, pp 273−345 and 699−749, John Wiley & Sons, Inc., New York.
36. Frieden, C. (1959) Glutamic dehydrogenase. III. The order of substrate addition in the enzymatic reaction, *J. Biol. Chem. 234*, 2891−2896.
37. Fromm, H. J. (1967) The use of competitive inhibitors in studying the mechanism of action of some enzyme systems utilizing three substrates, *Biochim. Biophys. Acta 139*, 221−230.
38. Rudolph, F. B. (1979) Product inhibition and abortive complex formation, *Methods Enzymol. 63*, 411−436.
39. Kaczka, E. A., Gitterman, C. O., Dulaney, E. L., and Folkers, K. (1962) Hadacidin, a new growth-inhibitory substance in human tumor systems, *Biochemistry 1*, 340−343.
40. Shigeura, H. T., and Gordon, C. N. (1962) Hadacidin, a new inhibitor of purine biosynthesis, *J. Biol. Chem. 237*, 1932−1936.
41. Shigeura, H. T., and Gordon, C. N. (1962) The mechanism of action of hadacidin. *J. Biol. Chem. 237*, 1937−1940.
42. Clark, A. W., and Rudolph, F. B. (1976) Regulation of purine metabolism. Adenylosuccinate synthetase from Novikoff ascites tumor cells, *Biochim. Biophys. Acta 437*, 87−90.
43. Markham, G. D., and Reed, G. H. (1977) Adenylosuccinate synthetase from *Azotobacter vinelandii*: purification, properties and steady-state kinetics, *Arch. Biochem. Biophys. 184*, 24−35.
44. Matsuda, Y., Shimura, K., Shiraki, H., and Nakagawa, H. (1980) Purification and properties of adenylosuccinate synthetase from Yoshida sarcoma ascites tumor cells, *Biochim. Biophys. Acta 616*, 340−350.
45. Jayalakshmi, R., Sumathy, K., and Balaram, H. (2002) Purification and characterization of recombinant *Plasmodium falciparum* adenylosuccinate synthetase expressed in *Escherichia coli*, *Protein Expression Purif. 25*, 65−72.
46. Ogawa, H., Shiraki, H., Matsuda, Y., Kakiuchi, K., and Nakagawa, H. (1977) Purification, crystallization, and properties of adenylosuccinate synthetase from rat skeletal muscle, *J. Biochem. (Tokyo) 81*, 859−869.
47. Stayton, M. M., Rudolph, F. B., and Fromm, H. J. (1983) Regulation, genetics, and properties of adenylosuccinate synthetase: a review, *Curr. Top. Cell Regul. 22*, 103−141.
48. Cleland, W. W. (1979) Substrate inhibition, *Methods Enzymol. 63*, 500−513.
49. Ogawa, H., Shiraki, H., and Nakagawa, H. (1976) Study on the regulatory role of fructose-1,6-diphosphate in the formation of AMP in rat skeletal muscle. A mechanism for synchronization of glycolysis and the purine nucleotide cycle, *Biochem. Biophys. Res. Commun. 68*, 524−528.
50. Lipps, G., and Krauss, G. (1999) Adenylosuccinate synthase from *Saccharomyces cerevisiae*: homologous overexpression, purification and characterization of the recombinant protein, *Biochem. J. 341*, 537−543.
51. Van der Weyden, M. B., and Kelly, W. N. (1974) Human adenylosuccinate synthetase. Partial purification, kinetic and regulatory properties of the enzyme from placenta, *J. Biol. Chem. 249*, 7282−7289.
52. Nagy, M., Djembo-Taty, M., and Heslot, H. (1973) Regulation of the biosynthesis of purine nucleotides in *Schizosaccharomyces pombe*. III. Kinetic studies of adenylosuccinate synthetase, *Biochim. Biophys. Acta 309*, 1−10.
53. Jahngen, E. G., and Rossomando, E. F. (1984) Adenylosuccinate synthetase from *Dictyostelium discoideum*: effects of hadacidin analogs and binding of [14C]hadacidin, *Arch. Biochem. Biophys. 229*, 145−154.
54. Garbers, D. L., Hardman, J. G., and Rudolph, F. B. (1974) Kinetic analysis of sea urchin sperm guanylate cyclase, *Biochemistry 13*, 4166−4171.
55. Iancu, C. V., Borza, T., Fromm, H. J., and Honzatko, R. B. (2002) IMP, GTP, and 6-phosphoryl-IMP complexes of recombinant mouse muscle adenylosuccinate synthetase, *J. Biol. Chem. 277*, 26779−26787.
56. Muirhead, K. M., and Bishop, S. H. (1974) Purification of adenylosuccinate synthetase from rabbit skeletal muscle, *J. Biol. Chem. 249*, 459−464.
57. Hou, Z., Wang, W., Fromm, H. J., and Honzatko, R. B. (2002) IMP alone organizes the active site of adenylosuccinate synthetase from *Escherichia coli*, *J. Biol. Chem. 277*, 5970−5976.
58. Gouet, P., Courcelle, E., Stuart, D. I., and Metoz, F. (1999) ESPript: multiple sequence alignments in PostScript, *Bioinformatics 15*, 305−308.
59. DeLano, W. L. (2002) The PyMOL Molecular Graphics System. http://www.pymol.org.

BI701009Y